Mechanistic Insights into Electrocatalytic Carbon— Bromine Bond Cleavage in Polybrominated Phenols

Eric C. R. McKenzie,^a Seyyedamirhossein Hosseini,^b Mayank Tanwar,^c Matthew Neurock,^{c,*}

Shelley D. Minteer,^b and Stephen C. Jacobson^{a,*}

^aDepartment of Chemistry, Indiana University, Bloomington, IN 47405, USA; ^bDepartment of Chemistry, University of Utah, Salt Lake City, UT 84112, USA; ^cDepartment of Chemical Engineering and Materials Science and Department of Chemistry, University of Minnesota,

Minneapolis, MN 55455, USA

*Corresponding authors. mneurock@umn.edu; jacobson@indiana.edu

Abstract. Carbon—halogen bond cleavage has been studied extensively for many years as a simple electrosynthesis step in the formation of more complex natural products. Reduction of halogenated phenols has received less attention, in part due to the lowered faradaic efficiency resulting from the competing hydrogen evolution reaction. Herein, we report the electroreduction of a series of brominated phenols through a homogeneous electrocatalytic (EC') mechanism. Beginning with the structurally simple 2-bromophenol, we use foot-of-thewave analysis to determine optimal catalysts. Nickel(II) salen requires the lowest overpotential

for C–Br reduction and was used across all substrates. Chronoamperometric studies and density functional theory calculations were carried out to contribute to our understanding of the reduction mechanism. Next, the more complex 2,6-dibromophenol and tetrabromobisphenol-A are studied by means of cyclic voltammetry, chronoamperometry, and density functional theory. Through analysis of molecular orbitals diagrams, the more complex brominated phenols are found to undergo sequential carbon–bromine bond reduction, wherein the electrogenerated radical species accepts a second electron to form a carbanion before second carbon–bromine bond cleavage occurs.

Keywords: Electrocatalysis, brominated phenols, cyclic voltammetry, chronoamperometry, density functional theory

Introduction

Phenols (and, more generally, flavonoids) are widely recognized as important moieties in medicinally active natural products.¹ Indeed, compounds such as caespitate, catechin, licochalcone A, and myricetin (Figure 1) exhibit anticancer, antimalarial, and antioxidant properties.^{2–5} While popular due to their natural abundance, chemical synthesis of these compounds often involves toxic solvents, expensive reagents, and long reaction times.⁶ Electrosynthesis provides a greener, faster, and less expensive alternative to carry out organic transformations under milder conditions.⁷

Figure 1. Naturally occurring phenolic organic products. **(a)** Caespitate, antibacterial; **(b)** catechin, antioxidant; **(c)** licochalcone A, anticancer; and **(d)** myricetin, antioxidant.

To date, our laboratory has examined extensively⁸⁻¹⁴ the reductive properties of carbon-halogen bond cleavage, as this process provides a relatively simple step toward the electrosynthesis of more complex species. In the case of simple aromatic halides, electron transfer at inert electrodes occurs through a well-understood mechanism involving an aryl radical intermediate; the reduction potential of this intermediate is often more positive than the original aryl halide, which results in a second electron transfer to form an aryl carbanion.¹⁵ If the reduction potential of the aryl radical is more negative than the original aryl halide, the radical species may abstract a hydrogen atom from a solvent molecule through hydrogen atom transfer (HAT). Alternatively, the carbanion can receive a proton from an adventitious water molecule or any suitable proton donor in solution.¹⁵ Recently, our laboratory has moved towards the investigation of more complex substrates with varying functional groups, such as

acetamides,^{16–18} esters,^{19,20} and aldehydes.²¹ However, the electrochemical behavior of halogenated phenolic compounds has not been widely studied.^{22–25} The moderate acidity of these species leads to enhanced hydrogen evolution with the increased concentration of protons in solution; as a result, the faradaic efficiency of dehalogenation is significantly lowered. Moreover, radical and carbanion intermediates generated throughout electrolysis are quite unstable, because aromaticity is disrupted.

From an environmental perspective, the electroreduction of halophenols is of particular interest also, as several of these compounds, such as pentachlorophenol, are viewed as probable carcinogens by the EPA. Others (e.g., 2,4,5-trichlorophenol) are known precursors to carcinogenic dioxins throughout the War. 2,3,7,8-(Figure 2a); Vietnam tetrachlorodibenzodioxin (TCDD) was found to be a significant contaminant in Agent Orange, which gave rise to unprecedented health problems in exposed individuals.²⁶ Furthermore, polyhalogenated phenols are structurally similar to thyroid hormones, particularly T₃ and T₄ (Figure 2b); as a result, several of these compounds are known to be endocrine disruptors. 27,28 This issue becomes exceptionally problematic, as many environmental pollutants can be metabolically hydroxylated, especially those which incorporate phenyl rings.²⁷ In addition to providing a straightforward mechanistic step in the synthesis of natural products with phenolic moieties, electroreduction also serves as a method of environmental remediation of these harmful reagents.

Figure 2. (a) Synthetic route of 2,3,7,8-tetrachlorodibenzodioxin (TCDD) from 2,4,5-trichlorophenol (245T).²⁶ TCDD is a major impurity in the manufacturing of 245T, which comprised 50% of the herbicide Agent Orange. **(b)** Thyroid hormones 3,3',5,5'-tetraiodo-L-thyroxin (T₄, left) and 3,3',5-triiodo-L-thyronine (T₃, right). Each structure contains a halogenated phenol moiety.

Herein, we report the systematic investigation of polybrominated phenol reduction by means of various homogeneous electron-transfer catalysts at carbon cathodes. Mediated carbon-bromine cleavage via an electrocatalyst features numerous advantages, such as applying less negative potentials and avoiding working electrode passivation. Our research group has achieved considerable success in the implementation of cobalt- and nickel-salen complexes to drive carbon-halogen bond cleavage at milder potentials.^{29–32} First, electroreduction of 2-bromophenol via nickel(II) salen, anthracene, and trans-stilbene was analyzed by means of cyclic voltammetry (CV) and constant-potential (bulk) electrolysis

(CPE). Results indicate that Ni(II) salen is the optimal catalyst for reduction of the carbon-bromine bond. Next, the electrolysis of 2,6-dibromophenol was performed with Ni(II) salen as the electrocatalyst. The mechanism of carbon-bromine cleavage in 2,6-dibromophenol was investigated through coulometric analysis and isotope incorporation studies via high-resolution gas chromatography-mass spectrometry (hi-res GC-MS). Electroreduction of tetrabromobisphenol-A (TBBPA) was then studied with CV and CPE. GC-MS was utilized to separate, identify, and quantitate products obtained from CPE of TBBPA in the presence of 1,1,1,3,3,3-hexaflouroisopropanol (HFIP) as the proton donor. Finally, first-principles density functional theory (DFT) calculations were carried out to gain mechanistic insights into the mediated reduction of the three substrates, which show excellent agreement with the experiments for the proposed mechanism. The sequential mechanism of TBBPA electroreduction was further unraveled by means of frontier molecular orbital analyses.

Methods

Materials. All of the following compounds were purchased from the indicated supplier and used without further purification: 2-bromophenol (Oakwood), 2,6-dibromophenol (99%, Sigma-Aldrich); 3,3',5,5'-tetrabromobisphenolA (TBBPA, 97%, Sigma-Aldrich); phenol (99+%, Sigma-Aldrich); bisphenol A (BPA, ≥99%, Sigma-Aldrich); [[2,2'-[1,2-ethanediylbis(nitrilomethylidyne)]bis[phenolato]]*N,N',O,O'*] nickel(II) (nickel(II) salen, 98%, Sigma-Aldrich); anthracene (96%, EM); trans-stilbene (96%, Sigma-Aldrich); 1,1,1,3,3,3-hexafluoroisopropanol (99%, Matrix Scientific); 1,1,1,3,3,3-hexafluoroisopropanol—OD (98

atom %D, Sigma-Aldrich); deuterium oxide (99.9 atom %D, Sigma-Aldrich); hexadecane (99%, Sigma-Aldrich); *N*,*N*-dimethylformamide (DMF, 99.9%, EMD Millipore Corporation); ethyl acetate (99.5%, Fisher); sodium chloride (Macron); sulfuric acid (>51% in water, Macron); sodium sulfate (99%, VWR). Tetramethylammonium tetrafluoroborate (TMABF₄, 98%, TCI) was recrystallized from water and methanol. Ultrahigh purity argon gas was purchased from Airgas.

Cyclic Voltammetry. All experiments were carried out in a one-compartment cell containing 0.1 M TMABF4–DMF. Working electrodes were made by press-fitting a glassy carbon rod into a machined Teflon tube to obtain an exposed area of 0.071 cm²,³³ These electrodes were polished with 0.05-μm alumina prior to each scan. A platinum coil served as the counter electrode, and the reference electrode consisted of a cadmium-mercury amalgam (Cd/Hg), which has a potential of –0.76 V vs. a saturated calomel electrode (SCE) at 25 °C.³⁴⁻³⁵ This reference is manufactured by filling a glass body with DMF saturated with NaCl and CdCl₂. Elemental Hg is then added to cover the Pt connection wire. A layer of Cd–Hg amalgam is added to the top of the elemental Hg, followed by a layer of NaCl and a layer of CdCl₂. Solutions were sparged with argon for 20 min prior to analysis to remove oxygen. All voltammograms reported herein are plotted in IUPAC convention. Potentials were initially set to 0 V, scanned cathodically to the switching potential, then returned to 0 V.

Bulk Electrolysis. For bulk electrolysis experiments, a reticulated vitreous carbon (130 cm² approximate surface area) served as the working electrode, a graphite rod served as the counter electrode, and the same reference electrode for cyclic voltammetry was utilized.³⁶ To each

electrochemical cell, 50 mM 1,1,1,3,3,3-hexafluoroisopropanol (HFIP) per bromine atom present was added to the solution as a source for either proton or hydrogen atom transfer.³⁷ Each electrolyzed sample contained a 10-µL hexadecane internal standard for quantitation purposes. For electrolyses involving deuterated regents, DMF was dried extensively by means of a solvent purification system (Pure Process Technology). The solvent-supporting electrolyte was stored on activated 3 Å sieves prior to use.

Electrolysis products were partitioned between ethyl acetate, brine, and 1 M sulfuric acid. The ethyl acetate layer was collected and then dried over anhydrous sodium sulfate. The method of internal standards and peak area normalization were used for quantitation by means of an Agilent 6890N gas chromatograph, equipped with a 15 m \times 0.25 mm capillary column with a DB-5 (5% phenylpolysiloxane, 95% methylpolysiloxane) stationary phase. This chromatograph was coupled to an Agilent 5973 inert mass-selective detector with an electronimpact source (70 eV).

Density Functional Theory Calculations. First-principles density functional theory (DFT) calculations were carried out herein using the Gaussian 16 software package³⁸ with the M06-L, M06 and M06-2X exchange-correlation functionals,³⁹ Stuttgart/Dresden effective core potentials with SDD basis set for Ni atom,⁴⁰ and 6-311++G(d,p) basis set⁴¹ for the remaining atoms. A systematic evaluation of the different functionals was carried out to justify the choice of the M06-L functional and is provided in the Supporting Information. The SMD (solvation model based on density) implicit solvation model was utilized to approximate the effects of the

DMF solvent.⁴² Additional computational details are further provided in the Supporting Information.

Results and Discussion

Direct reduction of 2-bromophenol at carbon cathodes and computational analysis. Several reports^{15,22,43,44} have described the reduction mechanism of aromatic halides at inert cathodes. Through either a stepwise (eq 1 and 2) or concerted (eq 3) process, the addition of one electron results in carbon–halogen bond cleavage and formation of an aryl radical. The reduction potential of the aryl radical is often more positive than the starting aryl halide, which results in a second electron transfer to form an aryl carbanion. Proton transfer from a protic solvent or a suitable proton donor in solution results in the dehalogenated product.

$$(1) ArX + e^- \rightleftharpoons ArX^-$$

$$(2) \qquad ArX^{-} \rightarrow Ar^{-} + X^{-}$$

(3)
$$ArX + e^{-} \rightarrow Ar \cdot + X^{-}$$

Figure 3 depicts a cyclic voltammogram for 5 mM 2-bromophenol at a glassy carbon working electrode scanned at 150 mV s⁻¹ in 0.1 M TMABF₄–DMF. A single, irreversible cathodic peak at –1.80 V vs. Cd/Hg is observed, which we ascribe to carbon–bromine bond cleavage. Indeed, controlled-potential electrolysis of 2-bromophenol at reticulated vitreous carbon cathodes biased to –1.80 V vs. Cd/Hg result in complete dehalogenation to phenol in quantitative yield with 2.06 electrons transferred per molecule of substrate. Additionally, deuterium incorporation studies with 200 mM D₂O result in roughly 56% deuterium incorporation.

Deuterium labeling, together with coulometric results, supports the notion of a two-electron cleavage pathway for the debromination of 2-bromophenol. We propose that the remaining 44% of product also forms via a two-electron pathway; however, the carbanion intermediate is likely quenched from the proton originating from 2-bromophenol itself.

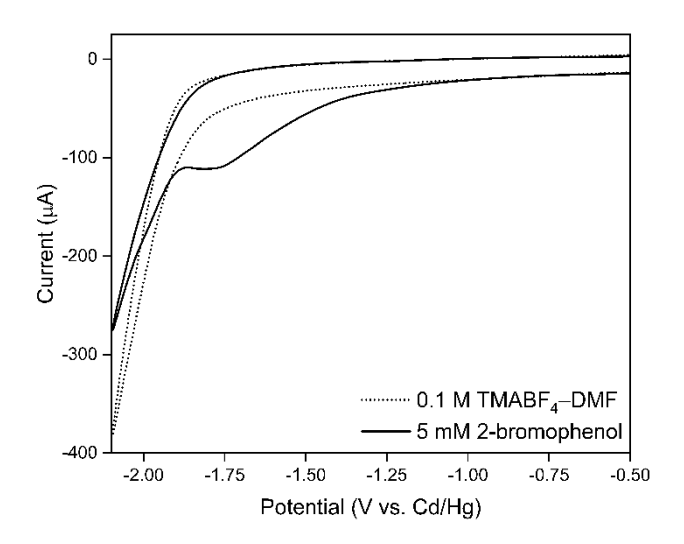


Figure 3. Cyclic voltammograms for O_2 -free 0.1 M TMABF₄–DMF (dotted black) and 5 mM 2-bromophenol in O_2 -free 0.1 M TMABF₄–DMF (solid black) obtained at a glassy carbon working electrode scanned at 150 mV s⁻¹.

Further, DFT calculations are largely supportive of the electrochemical results obtained by means of bulk electrolysis. As illustrated in Scheme 1, 2-bromophenol (1) accepts an electron at $E^0 = -1.59$ V vs. SHE (-1.07 V vs. Cd/Hg) to produce an aryl radical (1) and bromide ion through a concerted electron transfer mechanism. The reduction potential of 1 ($E^0 = -0.50$ V

vs. SHE or +0.02 V vs. Cd/Hg) is significantly more positive than the original substrate; hence the second electron transfer occurs rapidly to produce a carbanion intermediate (1^-), which is then quenched by protons in solution.

Scheme 1. Direct electroreduction of 2-bromophenol at carbon cathodes in dimethylformamide.

Br
$$\xrightarrow{e^{-}}$$
 OH $\xrightarrow{(vs. Cd/Hg)}$ OH $\xrightarrow{(vs. Cd/Hg)}$ OH $\xrightarrow{(vs. Cd/Hg)}$ OH $\xrightarrow{h^{+}}$ OH

Catalyst screening. Cyclic voltammetry was used to measure homogeneous electron-transfer rate constants between various electrocatalysts and 2-bromophenol to determine the best redox catalyst. Suitable electron-transfer catalysts must (1) exhibit fully reversible electron transfer in the absence of the substrate; (2) exhibit high turnover frequency (TOF) with the substrate; (3) have a reduction potential more positive than that of the substrate; and (4) have a standard reduction potential *more negative* than the standard reduction potential for reversible reduction of the substrate.²⁹ Given the criteria listed above, nickel(II) salen ($E^0 = -0.90 \text{ V}$ vs. Cd/Hg), anthracene ($E^0 = -1.13 \text{ V}$ vs. Cd/Hg), and trans-stilbene ($E^0 = -1.39 \text{ V}$ vs. Cd/Hg) were chosen to encompass the full catalytically acceptable potential range.¹⁵ Each catalyst exhibits complete reversibility within the required range and has been used previously

in carbon–halogen bond cleavage. ^{15, 29, 45} Further, DFT calculations predict a reduction potential of –0.96 V vs. Cd/Hg (–1.48 V vs. SHE) for nickel(II) salen, –1.25 V vs. Cd/Hg (–1.77 V vs. SHE) for anthracene, and –1.43 V vs. Cd/Hg (–1.95 V vs. SHE) for trans-stilbene, consistent with experimentally obtained potentials. A range of different M06 functionals was employed, and the corresponding potentials were compared against experiments to justify M06-L as the optimal choice of functional (Supporting Information). Additionally, calculations show that nickel(II) salen is a low-spin singlet and nickel(I) salen is a low-spin doublet complex.

To determine the most efficient catalyst, homogeneous electron transfer rate constants between each catalyst and substrate were measured. While a complete analysis of electron-transfer kinetics is quite complex, electron-transfer rate constants can be estimated by means of foot-of-the-wave analysis (FOWA). For a detailed explanation of FOWA, the interested reader is directed to the works of Savéant⁴⁶ and Dempsey.^{49,50} FOWA allows for determination of rate constants by means of eqs 4 and 5:^{49,51}

(4)
$$\frac{i}{i_p^0} = \frac{\frac{i_{pl}}{i_p^0}}{1 + \exp\left[\frac{F}{RT}(E - E_{cat/2}^0)\right]}$$

(5)
$$\frac{i_{pl}}{i_p} = 2.24 \sqrt{\frac{RTk_eC_A^0}{Fv}}$$

where i is the catalytic current of the substrate with catalyst, i_p^0 is the peak current of the catalyst in the absence of substrate, i_{pl} is the plateau current of the sigmoidal voltammogram associated with zone KS, E is the potential, $E_{cat/2}$ is the half-wave potential of the catalytic wave, v is the scan rate, k_e is the rate constant of homogeneous electron transfer, R is the universal gas

constant, T the temperature, and F is Faraday's constant. Plots of i/i_p^0 vs. $\left[1 + \exp\left[\frac{F}{RT}(E - E_{\text{cat/2}}^0)\right]\right]^{-1}$ result in a linear response where k_e can be extracted from the slope (Supporting Information).

Figure 4a displays voltammograms for 2 mM nickel(II) salen in the absence and presence of increasing concentrations of 2-bromophenol. As the concentration of 2-bromophenol increases, the cathodic peak grows in magnitude while the anodic peak current decreases. These experiments were repeated for anthracene and trans-stilbene (Figure S1, Supporting Information). These voltammograms were then used to determine the rate constant of electron transfer between the active form of the electrocatalyst and substrate by means of FOWA. Compiled in Table S1 (Supporting Information) are calculated electron-transfer rate constants between each catalyst and 2-bromophenol at 20, 50, 100, and 150 mV s⁻¹ and γ = 10. As illustrated, each catalyst appears to have a similar electron transfer rate constant to 2-bromophenol, differing only by a factor of 2.5. As a result, catalytic efficiencies ($i_0/i_p^{(0)}$) for each catalyst were also calculated. Trans-stilbene has the highest catalytic efficiency of C–Br cleavage in 2-bromophenol.

Once electron-transfer rate constants between catalyst and substrate were calculated, turnover frequencies (TOF) were determined by means of eq 6:46

(6)
$$TOF = \frac{k_e C_{AA}^0}{1 + \exp\left[\frac{F}{RT}\left(E - E_{PQ}^0\right)\right]}$$

Figure 4b depicts TOFs for each catalyst as a function of overpotential $(\eta = E - E_{2BrPhOH}^0)$ at glassy carbon cathodes scanned at 150 mV s⁻¹. In each case, y = 10 was utilized. Although transstilbene has the largest TOF, the process with nickel(II) salen has the lowest overpotential, with catalyzed reduction occurring near $\eta = 0$ mV. These data are further supported by bulk electrolysis of 5 mM 2-bromophenol in the presence of 2 mM nickel(II) salen at -1.00 V, as well as electrolysis of 5 mM 2-bromophenol and 2 mM trans-stilbene at -1.45 V. In each case, complete reduction to phenol is observed; however, electrolysis in the presence of nickel(II) takes longer than in the presence of trans-stilbene. DFT calculations show that the oneelectron reduction of 2-bromophenol is thermodynamically more favorable where the free energy of reaction for trans-stilbene ($\Delta G_{\text{reac}} = -35 \text{ kJ mol}^{-1}$) is more negative than anthracene $(\Delta G_{\text{reac}} = -18 \text{ kJ mol}^{-1})$ which is more negative than nickel(II) salen $(\Delta G_{\text{reac}} = 11 \text{ kJ mol}^{-1})$. This result is consistent with the largest TOF and shortest electrolysis time obtained experimentally with trans-stilbene followed by anthracene and nickel(II) salen. We further employed DFT calculations in conjunction with Marcus Theory to calculate electron-transfer barriers for the reduction of 2-bromophenol with the reduced form of these three catalysts. 47,48 Marcus theory gives free energy barriers for the reaction with trans-stilbene of $\Delta G^{\dagger} = 38 \text{ kJ mol}^{-1}$, anthracene of $\Delta G^{\dagger} = 45 \text{ kJ mol}^{-1}$, and nickel(II) salen of $\Delta G^{\dagger} = 67 \text{ kJ mol}^{-1}$ (Table 3 and Supporting Information). The kinetics of electron transfer follows the thermodynamics in all three cases, and the reactions occur in the normal regime of Marcus Theory ($|\Delta G_{\text{reac}}| < \lambda$, where λ is the reorganization energy). The nickel(II) salen was chosen as the optimal catalyst for the reduction of bromophenols as it had the lowest overpotential, and the duration of electrolysis was only minimally extended.

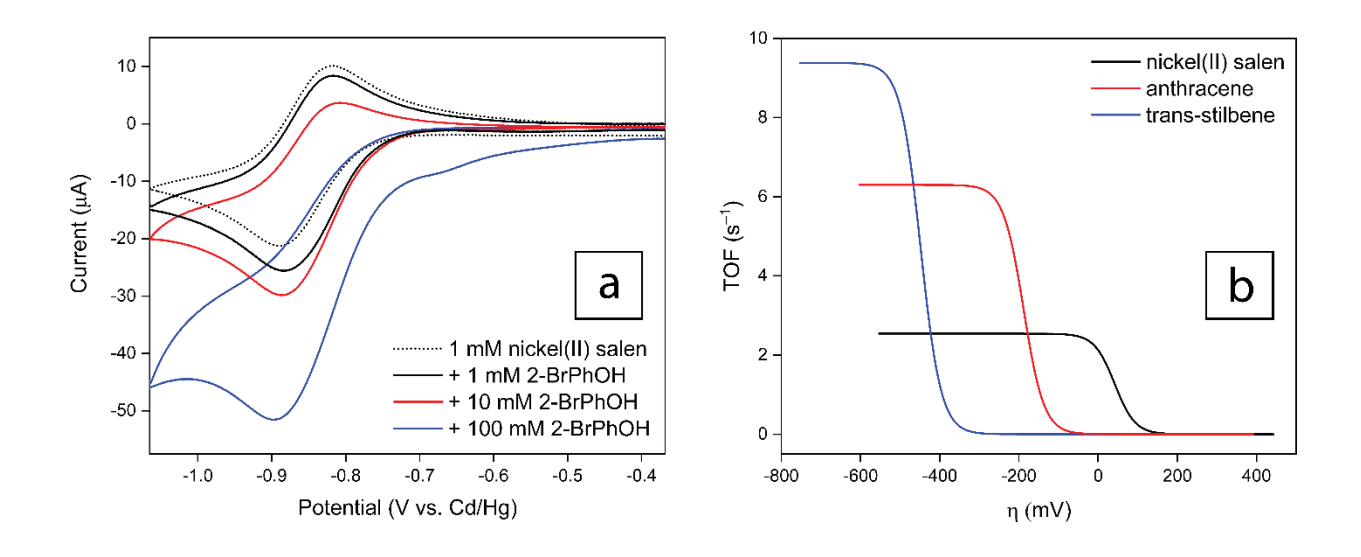


Figure 4. (a) Cyclic voltammograms for 1 mM nickel(II) salen (dotted black), and 1 mM nickel(II) salen in the presence of 1 mM (solid, black trace), 10 mM (solid red), and 100 mM (solid blue) 2-bromophenol at a glassy carbon working electrode scanned at 150 mV s⁻¹ in 0.1 M TMABF₄–DMF. (b) Turnover frequency (TOF) as a function of overpotential (η) for the catalyzed reduction of 2-BrPhOH by nickel(II) salen (solid black), anthracene (solid red), and trans-stilbene (solid blue). Recorded at a glassy carbon working electrode scanned at 150 mV s⁻¹ and an excess factor (γ) of 10.

Electrochemical behavior of 2,6-dibromophenol in the presence of Nickel(II) salen. With an optimal catalyst chosen, cyclic voltammetry of 2,6-dibromophenol was performed in the

absence and presence of nickel(II) salen. As shown in Figure 5a, direct reduction at carbon cathodes results in two irreversible cathodic peaks at -1.38 and -1.90 V vs. Cd/Hg. In the presence of nickel(II) salen (Figure 5b), an enhanced reduction peak is observed at -0.90 V vs. Cd/Hg, which grows with an increasing concentration of 2,6-dibromophenol. In contrast, the magnitude of the oxidative peak decreases. Interestingly, a second cathodic peak is present at ca. -1.30 V vs. Cd/Hg, which is both concentration and scan rate dependent (Figure S2a, Supporting Information).

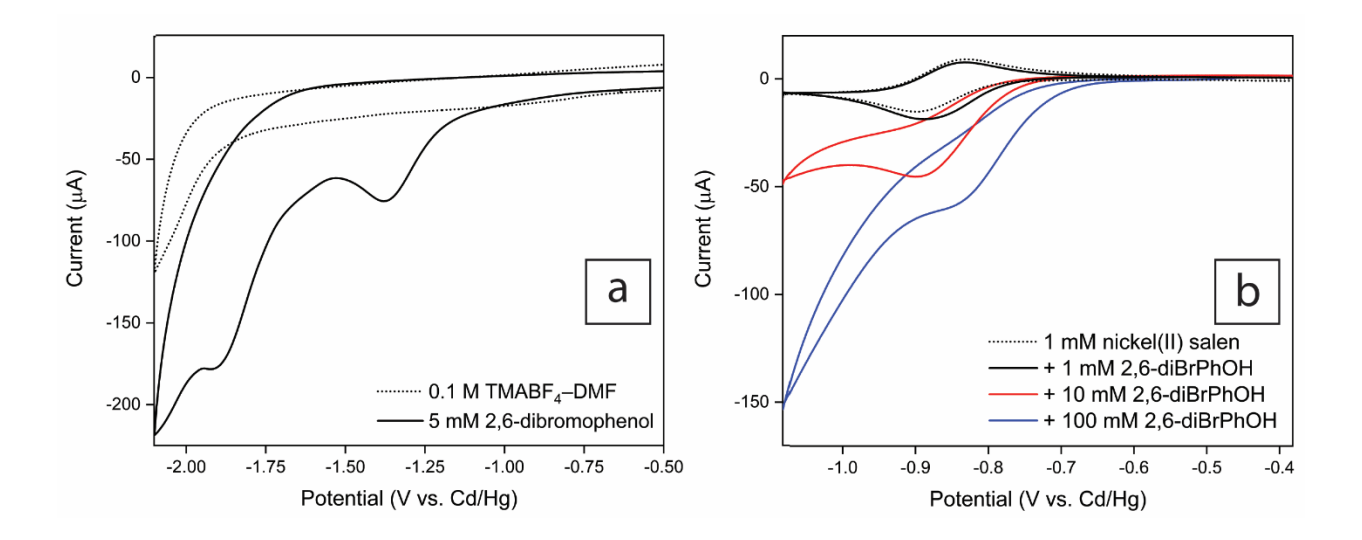


Figure 5. (a) Cyclic voltammograms for O₂-free 0.1 M TMABF₄–DMF (dotted black) and 5 mM 2,6-dibromophenol in O₂-free 0.1 M TMABF₄–DMF obtained at glassy carbon cathodes scanned at 150 mV s⁻¹. **(b)** Cyclic voltammograms for 1 mM nickel(II) salen (dotted black), and 1 mM nickel(II) salen in the presence of 1 mM (solid, black curve), 10 mM (solid red) and 100 mM (solid blue) 2,6-dibromophenol at glassy carbon cathodes scanned at 150 mV s⁻¹ in O₂-free 0.1 M TMABF₄–DMF.

Bulk electrolyses of 5 mM 2,6-dibromophenol in the presence of nickel(II) salen and excess HFIP were performed at reticulated vitreous carbon cathodes in 0.1 M TMABF4–DMF; Table 1 displays coulometric data and product distributions. At –1.00 V vs. Cd/Hg, electrolysis of 5 mM 2,6-dibromophenol in the presence of 2 mM nickel(II) salen produces 44% phenol and 23% 2-bromophenol, with approximately 20% unreacted starting material remaining. To discern radical and carbanion intermediates, we performed bulk reduction in the presence of excess deuterated HFIP (HFIP–OD). Mass spectrometric analysis of electrogenerated phenol reveals that roughly 91% has no deuterons incorporated, and only 9% has one deuteron incorporated. Moreover, of the 2-bromophenol generated, 94% has no deuterons incorporated and 6% has one deuteron incorporated.

Table 1. Coulometric data and product distributions for the reduction of 5 mM 2,6-dibromophenol at reticulated vitreous carbon cathodes in O₂-free DMF containing 0.10 M TMABF₄, 2 mM nickel(II) salen, and excess HFIP.

\overline{E}		Product Distribution (%) ^b					
(V vs. Cd/Hg)	II^{2}	2,6-diBrPhOH	BrPhOH	PhOH	Total		
-1.00	1.57	20	23	44	87		

^a Number of electrons per molecule of 2,6-dibromophenol

TR = trace amount; ND = not detected

^b Yield expressed as a percentage of initial substrate concentration

On the basis of voltammetric and chronoamperometric data, we propose the mechanism outlined in Scheme 2 for the bulk reduction of 2,6-dibromophenol in the presence of nickel(II) salen. At –1.00 V, nickel(II) salen accepts one electron to form the catalytically active nickel(I) salen (reaction [1]). DFT calculations predict a reduction potential of -0.96 V vs. Cd/Hg (-1.48 V vs. SHE) with a singlet d⁸ Ni(II) salen reducing to a doublet d⁹ Ni(I), consistent with the experimental value. This intermediate then transfers one electron to 2,6-dibromophenol where through a concerted mechanism, the carbon-bromine bond is cleaved to produce bromide and the aryl radical. The concerted carbon-bromine bond cleavage is observed with a calculated reduction potential of -0.95 V vs. Cd/Hg (-1.47 V vs. SHE). Moreover, Marcus Theory predicts a barrier of $\Delta G^{\dagger} = 61 \text{ kJ mol}^{-1}$ and reaction-free energy of $\Delta G_{\text{reac}} = -1 \text{ kJ mol}^{-1}$ for the first electron transfer step from the Ni(I) salen complex to form the aryl radical (reaction [2]) (Table 3 and Supporting Information). The kinetics of electron transfer follow the thermodynamics, and the reactions occur in the normal regime of Marcus Theory $(|\Delta G_{\text{reac}}| < \lambda$, where λ is the reorganization energy). This aryl radical can either abstract a hydrogen atom from the secondary carbon of HFIP (reaction [3], major pathway) or accept another electron from another nickel(I) salen complex to form the aryl carbanion (reaction [3], minor pathway). The aryl carbanion is then quenched by the proton originating from HFIP. The major pathway involves quenching of the radical through hydrogen atom transfer from excess HFIP in solution and is evident in deuterium incorporation studies, which show that over 90% of the phenol produced has no deuterium atoms incorporated when HFIP-OD

is utilized. Calculations show that, following the first electron transfer and carbon-bromine cleavage, the second electron transfer, if it occurs, will not lead to the cleavage of the second carbon-bromine bond. Hence, the aryl radical either abstracts a hydrogen atom or forms an aryl carbanion and accepts a proton. Transition state calculations further show a barrier of $\Delta G^{\dagger} = 30 \text{ kJ mol}^{-1}$ for hydrogen atom abstraction from HFIP by the aryl radical. With Marcus Theory, the homogeneous electron transfer barrier between the Ni(I) salen complex and the aryl radical substrate is $\Delta G^{\dagger} = 0$ kJ mol⁻¹ (Table 3 and Supporting Information). This reaction, however, occurs in the inverted regime of Marcus Theory ($|\Delta G_{\rm reac}| > \lambda$, where λ is the reorganization energy). While the kinetic barriers suggest that the hydrogen atom transfer pathway will not be favored over the aryl carbanion formation pathway, the excess concentration of HFIP may drive the hydrogen atom transfer pathway. With the excess concentration, the radical species encounters an HFIP molecule first rather than a Ni(I) salen complex. This will lead to the hydrogen atom transfer pathway, consistent with the deuterium labeling experiments.

Scheme 2. Nickel(I) salen-catalyzed electroreduction of 2,6-dibromophenol at carbon cathodes in dimethylformamide.

Nickel(I) salen-catalyzed reduction of tetrabromobisphenol-A (TBBPA). With the insights established from the bulk reduction of 2,6-dibromophenol, we decided to investigate the electrochemical behavior of TBBPA. Figure 6a shows a cyclic voltammogram for 5 mM TBBPA at a glassy carbon cathode scanned at 150 mV s⁻¹. Similar to 2,6-dibromophenol, two cathodic peaks are observed at −1.37 and −1.87 V vs. Cd/Hg. Voltammograms for 1 mM nickel(II) salen in the absence and presence of increasing concentrations of TBBPA at carbon cathodes scanned at 150 mV s⁻¹ are depicted in Figure 6b. When substrate is added to solution,

similar behavior to that of 2,6-dibromophenol is observed once again: where there is an increase in cathodic current at -0.90 V vs. Cd/Hg as substrate is added to the solution and a second cathodic peak at -1.29 V vs. Cd/Hg, which grows rapidly in comparison to the first peak as concentration and scan rate are increased (Figure S2a, Supporting Information). Moreover, as the concentration of substrate is increased, the magnitude of the anodic peak decreases.

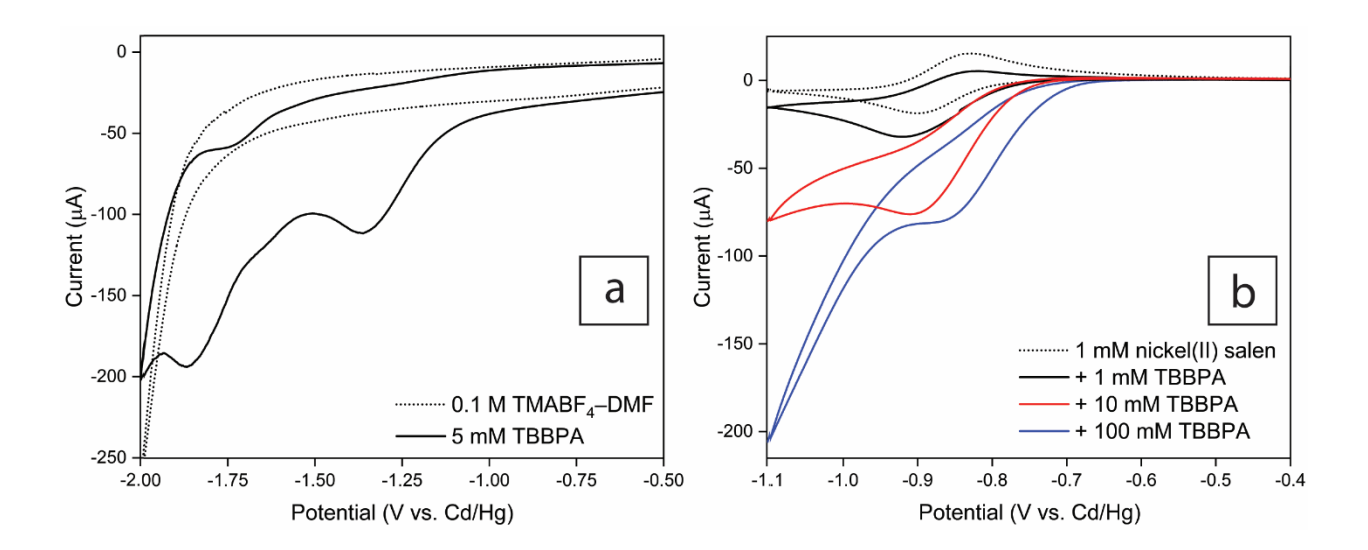


Figure 6. (a) Background cyclic voltammogram (dotted black) and cyclic voltammogram for 5 mM TBBPA (solid black) at a glassy carbon cathode scanned at 150 mV s⁻¹ in 0.1 M TMABF₄–DMF. **(b)** Cyclic voltammograms for 1 mM nickel(II) salen (dotted black) and 1 mM nickel(II) salen in the presence of 1 mM (solid black), 10 mM (solid red), and 100 mM (solid blue) TBBPA at glassy carbon cathodes scanned at 150 mV s⁻¹ in 0.1 M TMABF₄–DMF.

Controlled-potential electrolysis of 5 mM TBBPA was performed in the presence of 2 mM nickel(II) salen and excess HFIP at carbon cathodes biased to -1.00 V vs. Cd/Hg. Product distributions obtained (Table 2) show BPA as the major product, with 51% of starting material completely dehalogenated. Monobromobisphenol-A is present with 43% yield, whereas 6% dibromobisphenol-A was detected. Due to a lack of internal standards, the method of peak area normalization was used for quantitation instead of the method of internal standard. Overall, roughly 2.30 electrons are transferred per molecule of substrate, slightly lower than the 3.45 electrons that would coincide with the product distribution obtained. This difference highlights the uncertainty in the quantitation method employed. When HFIP–OD is utilized in place of HFIP, 87% of the BPA that is generated does not have deuterons incorporated, and only 12% of BPA has one deuteron incorporated. Thus, we conclude that the reduction of TBBPA by means of electrogenerated nickel(I) salen occurs through a one-electron mechanism to form a radical intermediate.

Table 2. Coulometric data and product distributions for the reduction of 5 mM TBBPA at reticulated vitreous carbon cathodes in oxygen-free DMF containing 0.10 M TMABF₄, 2 mM nickel(II) salen, and excess HFIP.

\overline{E}	II^{2}	Product Distribution (%) ^b					
(V vs. Cd/Hg)		TBBPA	Tri-	Di-	Mono-	BPA	Total
-1.00	2.30	ND	TR	6	43	51	100

^a Number of electrons transferred per molecule of TBBPA

^b Yield expressed as an area percentage of total peaks present in the chromatogram

TR = trace amount; ND = not detected

Results obtained for the catalyzed electroreduction of TBBPA at carbon cathodes suggest that the reduction proceeds in a mechanism that is similar to that proposed in Scheme 2 for the bulk reduction of 2,6-dibromophenol. At carbon cathodes biased to -1.00 V vs. Cd/Hg, nickel(II) salen is reduced to nickel(I) salen which subsequently transfers one electron to the substrate, resulting in carbon-bromine bond cleavage to produce a radical intermediate. Similar to the previous substrates, theoretical results show that the electron transfer occurs with a concerted carbon-bromine bond cleavage. Marcus Theory predicts a free energy barrier of $\Delta G^{\dagger} = 48 \text{ kJ mol}^{-1}$ and reaction-free energy of $\Delta G_{\text{reac}} = -2 \text{ kJ mol}^{-1}$ for the first electron transfer step from the Ni(I) salen complex to form the aryl radical intermediate (Table 3 and Supporting Information). Consistent with the previous two substrates, the kinetics of electron transfer follow the thermodynamics, and the reaction occurs in the normal regime of Marcus Theory ($|\Delta G_{\text{reac}}| < \lambda$, where λ is the reorganization energy). Furthermore, the energetics of electron transfer in all three substrates are very similar, indicating little-to-no effect of multiple carbon-bromine bonds of these polybrominated phenols on the cleavage of one particular carbon-bromine bond. The aryl radical species that forms is subsequently quenched by the transfer of the secondary hydrogen from HFIP. Although most of the substrate is reduced by this pathway, computational data indicate that the reduction potential of the

radical intermediate species ($E^0 = +0.10 \text{ V}$ vs. Cd/Hg or -0.42 V vs. SHE) is much more positive than that of the original halide ($E^0 = -0.93 \text{ V}$ vs. Cd/Hg or -1.45 V vs. SHE). As a result, the radical species can accept another electron, generating a carbanion intermediate that accepts a proton from HFIP. This pathway is observed in the small amount of deuteron incorporation through bulk reduction in the presence of HFIP–OD.

In addition, calculations show a lower likelihood of the radical intermediate accepting a second electron leading to a second carbon-bromine bond cleavage, either in the same ring or the adjacent ring of TBBPA. This result is consistent with the previous observation with 2,6dibromophenol where two sequential electron-transfer carbon-bromine bond cleavages were not observed. As discussed previously, the substrate radical can either abstract a hydrogen atom from HFIP or undergo a second electron transfer to form an aryl carbanion. The homogeneous electron transfer barrier between the Ni(I) salen complex and the aryl radical substrate was calculated via Marcus Theory to be $\Delta G = 0 \text{ kJ mol}^{-1}$ (Table 3 and Supporting Information). This reaction, however, occurs in the inverted regime of Marcus Theory $(|\Delta G_{\text{reac}}| > \lambda$, where λ is the reorganization energy). Similar to 2,6-dibromophenol, transition state calculations and Marcus theory results indicate unfavorable hydrogen atom abstraction by the aryl radical over the second electron transfer step leading to an aryl carbanion that accepts a proton. As the barrier for hydrogen atom abstraction is higher with HFIP $(\Delta G^{\dagger} = 30 \text{ kJ mol}^{-1})$ than the reduction of aryl radical to the anion $(\Delta G^{\dagger} = 0 \text{ kJ mol}^{-1})$, the higher overall rate of hydrogen atom transfer must be the result of the excess concentration of HFIP. Table 3 summarizes the key DFT energetics for the three substrates for the different electron-transfer and H-atom transfer steps in the mechanism of these reductions with the Ni(I) salen catalyst.

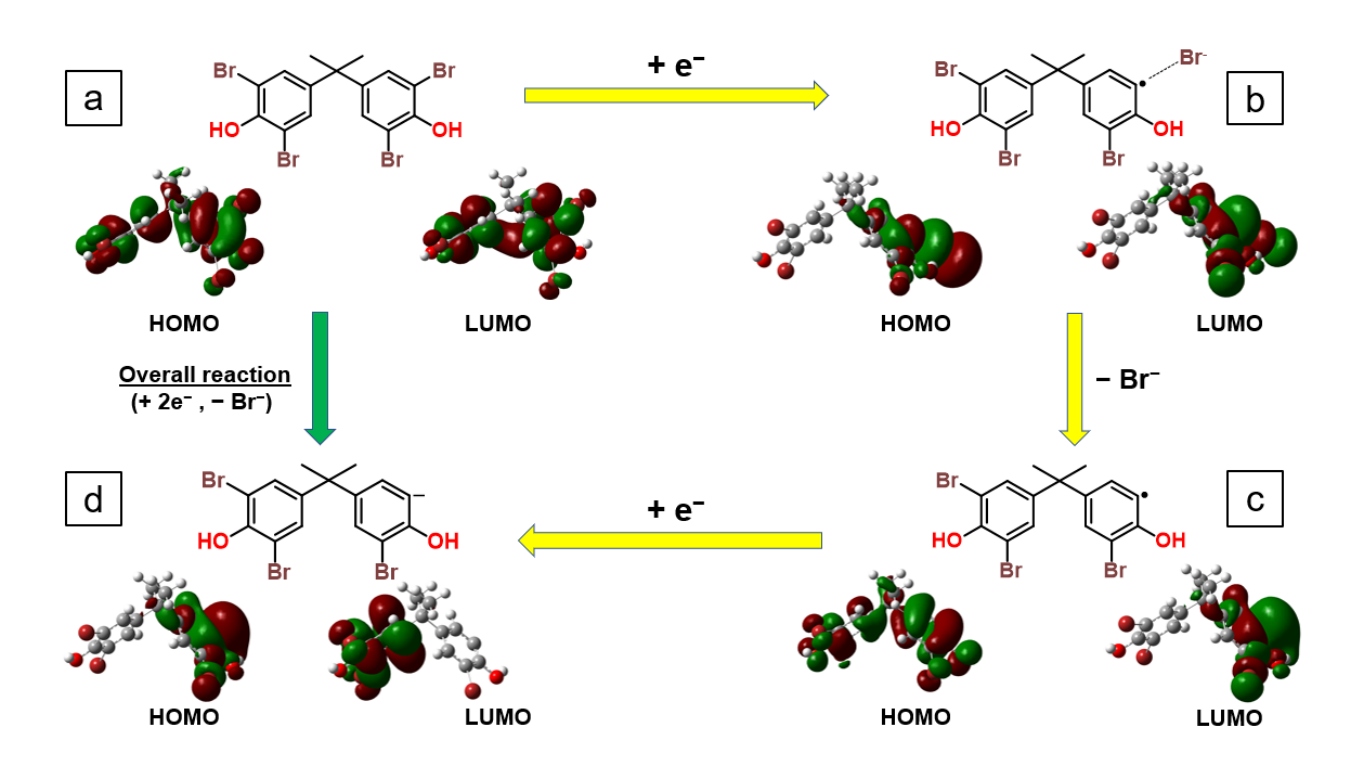
Table 3. Summary of DFT energetics for the three substrates with Ni(I) salen catalyst and HFIP.

	First electron reduction		Marcus	Second redu	Marcus	H atom transfer	
Substrate	ΔG^{\sharp} (kJ mol ⁻¹)	$\Delta G_{ m reac}$ (kJ mol $^{-1}$)	regime	ΔG^{t} (kJ mol ⁻ 1)	$\Delta G_{ m reac}$ (kJ mol ⁻¹)	regime	ΔG^{t} (kJ mol ⁻¹)
2-BrPhOH	67	11		2	-94		33
2,6- diBrPhOH	61	-1	normal	0	-110	inverted	30
TBBPA	48	-2	•	0	-101	•	30

As shown in Scheme 3, molecular orbital analysis shows that the highest occupied molecular orbital (HOMO) and the lowest unoccupied molecular orbital (LUMO) are initially delocalized over both TBBPA rings (structure a). Following the first concerted carbon–bromine cleavage in the anionic radical complex, the HOMO and LUMO become localized over the ring that carries the radical (structure b). After complete removal of the bromide ion from the radical intermediate, the HOMO becomes delocalized again over the two rings. However, the LUMO is still localized over the ring carrying the radical (structure c). This localization likely

prevents the second carbon–bromine cleavage from the adjacent ring. Upon a second electron transfer, which leads to formation of the carbanion, the HOMO becomes localized over the ring which carries the carbanion, and the LUMO now shifts to the adjacent ring (structure d). Thus, the results from the orbital analysis indicate that the first carbon–bromine cleavage occurs in one ring and does not propagate to the adjacent ring until the formation of the carbanion species (complete replacement of the carbon–bromine bond with a carbon–hydrogen bond). Only after carbanion formation does the LUMO shift to the adjacent ring, indicating that the second carbon–bromine bond cleavage will likely occur in the adjacent ring.

Scheme 3. Molecular orbital analysis for sequential electron transfers and carbon-halogen cleavage in TBBPA.



Conclusions

The electrocatalyzed reduction of a series of bromophenols was analyzed at carbon cathodes. Nickel(II) salen was determined to be the most energy-efficient catalyst for reduction, because the overpotential was lowest when compared to anthracene and trans-stilbene. Cyclic voltammograms for 2-bromophenol, 2,6-dibromophenol, and tetrabromobisphenol-A in the presence of nickel(II) salen show a single, irreversible cathodic peak. Bulk reduction of each in the presence of nickel(II) salen and HFIP show the completely dehalogenated species as the predominant product. On the basis of the data obtained, we propose that bromophenols are reduced through a one-electron mechanism, where nickel(II) salen is first reduced to nickel(I) salen (electrochemical step, E). Electrogenerated nickel(I) salen then transfers an electron to the bromophenol resulting in carbon-bromine bond cleavage and production of bromide and an aryl radical (electrocatalyzed step, C'). Density functional theory calculations show that the first electron-transfer step and carbon-bromine bond cleavage occur concertedly in all substrates. The aryl radical can either accept a hydrogen atom from the secondary carbon of HFIP or receive a second electron from nickel(I) salen generating a carbanion, which is quenched by the acidic proton on HFIP. Although calculations show that reduction to a carbanion is feasible, deuterium labeling experiments show that the hydrogen atom abstraction pathways are favored for the aryl radicals compared to the aryl carbanion formation pathways for all substrates, which must be the result of the excess concentration of HFIP employed in the experiments. Further, for substrates with multiple carbon-bromine

bonds, a second carbon–bromine bond cleavage occurs only after the first carbon–bromine bond has been completely reduced to a carbon–hydrogen bond. Hence, a sequential mechanism of carbon–bromine bond cleavage is proposed for mediated polybrominated phenol reduction involving an initial electron transfer accompanied by either a hydrogen atom abstraction step (more favorable) or a second electron-proton transfer step.

Supporting Information. Voltammograms for catalyst screening, voltammograms for 2,6-dibromophenol and tetrabromobisphenol-A at wider potential windows, and details of computational analysis. Supporting Information is available free of charge at https://pubs.acs.org.

Corresponding Authors

Stephen C. Jacobson – Department of Chemistry, Indiana University, Bloomington, Indiana 47405, United States, orcid.org/0000-0003-2415-041X; Email: jacobson@indiana.edu

Matthew Neurock – Department of Chemical Engineering and Materials Science and Department of Chemistry, University of Minnesota, Minneapolis, Minnesota 55455, United States, orcid.org/0000-0003-1458-7837; Email: mneurock@umn.edu

Authors

Eric C. R. McKenzie – Department of Chemistry, Indiana University, Bloomington, Indiana 47405, United States, orcid.org/0000-0002-8581-2774

Seyyedamirhossein Hosseini – Department of Chemistry, University of Utah, Salt Lake City, Utah 84112, United States, orcid.org/0000-0002-3617-2547

Mayank Tanwar – Department of Chemical Engineering and Materials Science, University of Minnesota, Minnesota, Minnesota 55455, United States, orcid.org/0000-0003-2205-6016.

Shelley D. Minteer – Department of Chemistry, University of Utah, Salt Lake City, Utah 84112, United States, orcid.org/0000-0002-5788-2249

Notes. (1) The authors declare no competing financial interest. (2) A data set collection of computational results is available in the ioChem-BD repository⁵² and can be accessed via https://doi.org/10.19061/iochem-bd-6-209 and includes density functional theory computational input and output data. Moreover, all data for product characterization, model parameters, and additional computational details can be found in the Supporting Information.

Acknowledgments. A majority of this study was performed under the tutelage of the late Dennis G. Peters (April 17, 1937–April 13, 2020). E.C.R.M. and S.C.J. thank the Department of Chemistry at Indiana University and the Dorothy & Edward Bair Chair in Chemistry for support. S.D.M., M.N., S.H., and M.T. acknowledge the National Science Foundation Center for Synthetic Organic Electrochemistry (CHE-2002158) for the generous funding. M.N. and M.T. acknowledge the Minnesota Supercomputing Institute (MSI) at the University of Minnesota for computational resources.

References

- (1) Hosseini, S.; Thapa, B.; Medeiros, M. J.; Pasciak, E. M.; Pence, M. A.; Twum, E. B.; Karty, J. A.; Gao, X.; Raghavachari, K.; Peters, D. G. Electrosynthesis of a Biaurone by Controlled Dimerization of Flavone: Mechanistic Insight and Large-Scale Application. *J. Org. Chem.* **2020**, *85*, 10658–10669.
- (2) Raab, T.; Barron, D.; Vera, F. A.; Crespy, V.; Oliveira, M.; Williamson, G. Catechin Glucosides: Occurrence, Synthesis, and Stability. *J. Agric. Food Chem.* **2010**, *58*, 2138–2149.
- (3) Jeon, J.-H.; Kim, M. R.; Jun, J.-G. Concise Synthesis of Licochalcone A through Water-Accelerated [3, 3]-Sigmatropic Rearrangement of an Aryl Prenyl Ether. *Synthesis* **2011**, *2011*, 370–376.
- (4) Liu, T.; Peng, F.; Cao, X.; Liu, F.; Wang, Q.; Liu, L.; Xue, W. Design, Synthesis, Antibacterial Activity, Antiviral Activity, and Mechanism of Myricetin Derivatives Containing a Quinazolinone Moiety. *ACS Omega* **2021**, *6*, 30826–30833.
- (5) Manion, D. Progress Towards the Total Synthesis of Caespitate: An Acylated Phloroglucinol. M.S. Thesis, Villanova University, Villanova, PA, **2020**.
- (6) McKenzie, E. C. R.; Hosseini, S.; Petro, A. G. C.; Rudman, K. K.; Gerroll, B. H. R.; Mubarak, M. S.; Baker, L. A.; Little, R. D. Versatile Tools for Understanding Electrosynthetic Mechanisms. *Chem. Rev.* **2022**, *122*, 3292–3335.
- (7) Yan, M.; Kawamata, Y.; Baran, P. S. Synthetic Organic Electrochemical Methods since 2000: On the Verge of a Renaissance. *Chem. Rev.* **2017**, *117*, 13230–13319.
- (8) Martin, E. T.; Strawsine, L. M.; Mubarak, M. S.; Peters, D. G. Direct Reduction of 1,2-and 1,6-Dibromohexane at Silver Cathodes in Dimethylformamide. *Electrochim. Acta* **2015**, *186*, 369–376.
- (9) Mubarak, M. S.; Peters, D. G., Electrochemical Reduction of 1,6-Dihalohexanes at Carbon Cathodes in Dimethylformamide. *J. Org. Chem.* **1995**, *60*, 681–685.
- (10) Raess, P. W.; Mubarak, M. S.; Ischay, M. A.; Foley, M. P. Jennermann, T. B.; Raghavachari, K.; Peters, D. G., *J. Electroanal. Chem.* **2007**, *603*, 124–134.
- (11) Mbarak, M. S.; Peters, D. G., Electrochemical Reduction of 2-Iodooctane and 2-Bromooctane at Mercury Cathodes in Dimethylformamide. *J. Org. Chem.* **1982**, *47*, 3397–3403.
- (12) McGuire, C. M.; Peters, D. G. Electrochemical Dechlorination of 4,4'-(2,2,2-Trichloroethane-1,1-Diyl)Bis(Chlorobenzene) (DDT) at Silver Cathodes. *Electrochim. Acta* **2014**, *137*, 423–430.
- (13) Mubarak, M. S.; Peters, D. G. Electrochemical Reduction of Di-, Tri-, and Tetrahalobenzenes at Carbon Cathodes in Dimethylformamide Evidence for a Halogen Dance During the Electrolysis of 1,2,4,5-Tetrabromobenzene. *J. Electroanal. Chem.* **1997**, *435*, 47–53.
- (14) Peverly, A. A.; Pasciak, E. M.; Strawsine, L. M.; Wagoner, E. R.; Peters, D. G. Electrochemical Reduction of Decabromodiphenyl Ether at Carbon and Silver Cathodes in Dimethylformamide and Dimethyl Sulfoxide. *J. Electroanal. Chem.* **2013**, 704, 227–232.
- (15) Andrieux, C. P.; Blocman, C.; Dumas-Bouchiat, J. M.; Savéant, J.-M. Heterogeneous and Homogeneous Electron Transfers to Aromatic Halides. An Electrochemical Redox Catalysis Study in the Halobenzene and Halopyridine Series. *J. Am. Chem. Soc.* **1979**, *101*, 3431–3441.
- (16) Petro, A. G. C.; Mubarak, M. S.; Peters, D. G. Electrochemical Reduction of 2-Halo-N-Phenylacetamides at Glassy Carbon Cathodes in Dimethylformamide. *J. Electroanal. Chem.* **2019**, 840, 456–461.

- (17) Petro, A. G. C.; Thapa, B.; Karty, J. A.; Raghavachari, K.; Baker, L. A.; Peters, D. G. Direct Electrochemical Reduction of Acetochlor at Carbon and Silver Cathodes in Dimethylformamide. *J. Electrochem. Soc.* **2020**, *167*, 155517.
- (18) Pasciak, E. M.; Sengupta, A.; Mubarak, M. S.; Raghavachari, K.; Peters, D. G. Electrochemical Reduction of 2-Chloro-N-Phenylacetamides at Carbon and Silver Cathodes in Dimethylformamide. *Electrochim. Acta* **2014**, *127*, 159–166.
- (19) Pasciak, E. M.; Peters, D. G. Reduction of Substituted Phenyl 2-Chloroacetates at Silver Cathodes: Electrosynthesis of Coumarins. *J. Electrochem. Soc.* **2014**, *161*, G98–G102.
- (20) Pasciak, E. M.; Rittichier, J. T.; Chen, C.-H.; Mubarak, M. S.; VanNieuwenhze, M. S.; Peters, D. G. Electroreductive Dimerization of Coumarin and Coumarin Analogues at Carbon Cathodes. *J. Org. Chem.* **2015**, *80*, 274–280.
- (21) Hosseini, S.; Bawel, S. A.; Mubarak, M. S.; Peters, D. G. Rapid and High-Yield Electrosynthesis of Benzisoxazole and Some Derivatives. *ChemElectroChem* **2019**, *6*, 4318–4324.
- (22) Knust, K. N.; Foley, M. P.; Mubarak, M. S.; Skljarevski, S.; Raghavachari, K.; Peters, D. G., *J. Electroanal. Chem.* **2010**, *638*, 100–108.
- (23) Xu, Y.; Zhu, Y.; Zhao, F.; Ma, C. Electrocatalytic Reductive Dehalogenation of Polyhalogenated Phenols in Aqueous Solution on Ag Electrodes. *Appl. Catal.*, A **2007**, 324, 83–86.
- (24) Rondinini, S.; Mussini, P. R.; Specchia, M.; Vertova, A. The Electrocatalytic Performance of Silver in the Reductive Dehalogenation of Bromophenols. *J. Electrochem. Soc.* **2001**, *148*, D102–D107.
- (25) Chetty, R.; Christensen, P. A.; Golding, B. T. In situ FTIR studies on the electrochemical reduction of halogenated phenols. *Chemical Commun.* **2003**, 984–985.
- (26) Klaassen, C. D. Casarett & Doull's Toxicology the Basic Science of Poisons; McGraw-Hill Education: New York, 2013.
- (27) Montaño, M.; Gutleb, A. C.; Murk, A. J. Persistent Toxic Burdens of Halogenated Phenolic Compounds in Humans and Wildlife. *Environ. Sci. Technol.* **2013**, *47*, 6071–6081.
- (28) Suzuki, G.; Takigami, H.; Watanabe, M.; Takahashi, S.; Nose, K.; Asari, M.; Sakai, S. Identification of Brominated and Chlorinated Phenols as Potential Thyroid-Disrupting Compounds in Indoor Dusts. *Environ. Sci. Technol.* **2008**, *42*, 1794–1800.
- (29) Martin, E. T.; McGuire, C. M.; Peters, D. G. Catalytic Reduction of Organic Halides by Electrogenerated Nickel (I) Salen. *Electrochem. Soc. Interface* **2016**, *25*, 41.
- (30) Alleman, K. S.; Peters, D. G., Catalytic Reduction of Iodoethane by Cobalt (I) Salen Electrogenerated at Vitreous Carbon Cathodes. *J. Electroanal. Chem.* **1998**, *451*, 121–128.
- (31) Gach, P. C.; Karty, J. A.; Peters, D. G. Catalytic Reduction of Hexachlorobenzene and Pentachlorobenzene by Cobalt (I) Salen Electrogenerated at Vitreous Carbon Cathodes in Dimethylformamide. *J. Electroanal. Chem.* **2008**, *612*, 22–28.
- (32) Gach, P. C.; Mubarak, M. S.; Karty, J. A.; Peters, D. G. Catalytic Reduction of 4, 4'-(2, 2, 2-Trichloroethane-1, 1-Diyl) Bis (Chlorobenzene) with Cobalt (I) Salen Electrogenerated at Vitreous Carbon Cathodes in Dimethylformamide. *J. Electrochem. Soc.* **2006**, *154*, F1.
- (33) Vieira, K. L.; Peters, D. G. Voltammetric Behavior of Tertiary Butyl Bromide at Mercury Electrodes in Dimethylformamide. *J. Electroanal. Chem.* **1985**, *196*, 93–104.
- (34) Hall, J. L.; Jennings, P. W. Modification of the preparation of a cadmium amalgam reference electrode for use in N,N-dimethylformamide. *Anal. Chem.* **1976**, *48*, 2026–2027.
- (35) Marple, L. W. Reference Electrode for Anhydrous Dimethylformamide. *Anal. Chem.* **1967**, 39, 844–846.

- (36) Vanalabhpatana, P.; Peters, D. G. Catalytic Reduction of 1,6-Dihalohexanes by Nickel(I) Salen Electrogenerated at Glassy Carbon Cathodes in Dimethylformamide. *J. Electrochem. Soc.* **2005**, *152*, E222–E229.
- (37) Rudman, K. K.; Thapa, B.; Tapash, A.; Mubarak, M. S.; Raghavachari, K.; Hosseini, S.; Minteer, S. D. Mechanistic Studies of the Electrocatalytic Carbon–Bromine Cleavage and the Hydrogen Atom Incorporation from 1,1,1,3,3,3-Hexaflouroisopropanol. *J. Electrochem. Soc.* **2022**, *169*, 115502.
- (38) Frisch, M.; Trucks, G. W.; Schlegel, H. B.; Scuseria, G. E.; Robb, M. A.; Cheeseman, J. R.; Scalmani, G.; Barone, V.; Mennucci, B.; Petersson, G. Gaussian 09, Revision D. 01. Gaussian, Inc., Wallingford CT: 2009.
- (39) Zhao, Y.; Truhlar, D. G. A New Local Density Functional for Main-Group Thermochemistry, Transition Metal Bonding, Thermochemical Kinetics, and Noncovalent Interactions. *J. Chem. Phys.* **2006**, *125*, 194101.
- (40) Dolg, M.; Wedig, U.; Stoll, H.; Preuss, H. Energy-Adjusted Abinitio Pseudopotentials for the First Row Transition Elements. *J. Chem. Phys.* **1987**, *86*, 866–872.
- (41) Hariharan, P. C.; Pople, J. A. Accuracy of AH*n* Equilibrium Geometries by Single Determinant Molecular Orbital Theory. *Mol. Phys.* **1974**, *27*, 209–214.
- (42) Marenich, A. V.; Cramer, C. J.; Truhlar, D. G. Universal Solvation Model Based on Solute Electron Density and on a Continuum Model of the Solvent Defined by the Bulk Dielectric Constant and Atomic Surface Tensions. *J. Phys. Chem. B* **2009**, *113*, 6378–6396.
- (43) Andrieux, C. P.; Saveant, J. M.; Su, K. B. Kinetics of Dissociative Electron Transfer. Direct and Mediated Electrochemical Reductive Cleavage of the Carbon–Halogen Bond. *J. Phys. Chem.* **1986**, *90*, 3815–3823.
- (44) Isse, A. A.; Mussini, P. R.; Gennaro, A. New Insights into Electrocatalysis and Dissociative Electron Transfer Mechanisms: The Case of Aromatic Bromides. *J. Phys. Chem. C* **2009**, *113*, 14983–14992.
- (45) Savéant, J.-M. Dissociative Electron Transfer. New Tests of the Theory in the Electrochemical and Homogeneous Reduction of Alkyl Halides. *J. Am. Chem. Soc.* **1992**, *114*, 10595–10602.
- (46) Costentin, C.; Drouet, S.; Robert, M.; Savéant, J.-M. Turnover Numbers, Turnover Frequencies, and Overpotential in Molecular Catalysis of Electrochemical Reactions. Cyclic Voltammetry and Preparative-Scale Electrolysis. *J. Am. Chem. Soc.* **2012**, *134*, 11235–11242.
- (47) Marcus, R. A. On the Theory of Oxidation-Reduction Reactions Involving Electron Transfer. I. *J. Chem. Phys.* **1956**, *24*, 966–978.
- (48) Bard, A. J.; Faulkner, L. F.; White, H. S. Electrochemical Methods: Fundamentals and Applications, 3rd ed.; Wiley, NewYork, **2022**.
- (49) Lee, K. J.; Elgrishi, N.; Kandemir, B.; Dempsey, J. L. Electrochemical and Spectroscopic Methods for Evaluating Molecular Electrocatalysts. *Nat. Rev. Chem.* **2017**, *1*, 0039.
- (50) Rountree, E. S.; McCarthy, B. D.; Eisenhart, T. T.; Dempsey, J. L. Evaluation of Homogeneous Electrocatalysts by Cyclic Voltammetry. *Inorg. Chem.* **2014**, *53*, 9983–10002.
- (51) Costentin, C.; Savéant, J.-M. Multielectron, Multistep Molecular Catalysis of Electrochemcal Reactions: Benchmarking of Homogeneous Catalysts. *ChemElectroChem* **2014**, 1, 1226–1236.
- (52) Álvarez-Moreno, M.; de Graaf, C.; Lopez, N.; Maseras, F.; Poblet, J.M.; Bo, C. *J. Chem. Inf. Model.* **2015**, 55, 95-103.

TOC Graphic